

Predicting the flowability of powder mixtures from their single components properties through the multi-component population-dependent granular Bond number; extension to ground powder mixtures

Martin GIRAUD^{a,b}, Stéphane VAUDEZ^b, Cendrine GATUMEL^a, Jeremy NOS^c, Thierry GERVAIS^d,
Guillaume BERNARD-GRANGER^b, Henri BERTHIAUX^a

^a Laboratoire RAPSODEE, UMR CNRS 5302, IMT Mines Albi, Campus Jarlard, 81013 Albi Cedex 09, France

^b CEA, DES, ISEC, DMRC, Université de Montpellier, Marcoule, France

^c Orano, 125 avenue de Paris, 92320 Châtillon, France

^d Orano Melox, Les Tourettes, D138A, 30200 Chusclan, France

Corresponding author: Henri BERTHIAUX^a – henri.berthiaux@mines-albi.fr

Abstract:

The granular Bond number, defined as the ratio between interparticle attractive forces and particle's weight, can be computed to predict the flow behavior of powders. Previous studies used this dimensionless number to predict the flowability of various pharmaceutical or ceramic powders, exhibiting polydispersed particle size distributions. In this paper, we employ a multi-component population-dependent granular Bond number in order to apply this model to powder mixtures. Some binary and ternary mixtures are prepared using two different techniques: a Turbula® mixer and a ball mill. The flowability predictions appear to be in very good agreement with the empirical measurements, carried out with a powder shear tester. However, the model parameters seem to be slightly different between milled and raw powders. The model discussed in this paper allows a prediction of the flowability of powder mixtures according to their composition and serve as a guide for product formulation and equipment design.

Keywords:

Powder rheology – powder mixtures – shear test – granular Bond number

Abbreviations:

AFM: Atomic force microscopy

DVS: Dynamic vapor sorption

SEM: Scanning electron microscopy

GB: Granular Bond number

PGB: Population dependent granular Bond number

MPGB: Multi-component population dependent granular Bond number

Glossary:

Notation	Parameter	Usual units
ρ	True density	g.cm^{-3}
γ^d	Dispersive surface energy	mN.m^{-1}
D_0	Cut off distance	nm
A	Hamaker constant	$10^{-19}.\text{J}$
d	Particle diameter	μm
d_{asp}	Particle asperity size	nm
z_0	Interparticle distance	Nm
g	Gravity constant	m.s^{-2}
w	Mass fraction of a powder mixture	-
z	Surface fraction of a powder mixture	-
$f_s(x)$	Surface fraction of size x	-
D	Sauter mean diameter	μm
$span$	Span distribution parameter	-
J	Pebbles filling ratio	-
U	Powder level	-
ε_g	Pebbles bed porosity	-

d	Pebbles diameter	mm
Fr	Froude number	-
ω	Rotational speed	rad.s ⁻¹
D	Diameter of the drum	mm
τ	Shear stress	kPa
σ	Normal stress	kPa
σ_c	Pre-consolidation stress	kPa
c	Cohesion parameter	kPa
φ	Angle of internal friction	°
μ	Friction coefficient	-
σ_1	Major consolidation stress	kPa
σ_3	Minor consolidation stress	kPa
f_c	Cohesion stress	kPa
ff_c	Flow function coefficient	-
F_{vdW}	Van der Waals force	μN
W	Weight	μN
Bo_g	Granular Bond number (GB)	-
Bo_G	Population dependent granular Bond number (PGB)	-
$Bo_{G,mix}$	Multi-component population dependent granular Bond number (MPGB)	-

1. Introduction

Particulate systems are commonly handled in most industries involving food, pigments, pharmaceutical and chemical compounds or minerals for example. Yet, the behavior of bulk powders is known to be highly unpredictable and may lead to production slowdown or equipment damaging if not handled with care. However, unlike fluid mechanics, the study of flow behavior of particulate solids has only been developed in recent years and remains not fully understood [1].

The poor flowing ability of some powders results from the force balance at particle scales. Indeed, under a certain size, generally considered around 100 μm , some attractive interparticle forces, such as the Van der Waals forces, start to overcome the weight contribution of the particles, resulting in a cohesive behavior of the powder at macroscopic scale [2]. Thus, some authors have attempted to establish a link between the bulk behavior of powders and the interparticle forces that depends on the particles properties. Li [3] has successfully compared the pull off force measured by atomic force microscopy (AFM) to the adhesion forces computed using the Rumpf's theory and commonly used Van der Waals force model taking into account particle properties such as shape, elasticity or plasticity. Then, he attempted to derive a model allowing a prediction of the flowability and the compactability of pharmaceutical powders from AFM measurements. Tomasetta [4] also built a model based on Rumpf's theory assuming elastic or plastic deformations. The model links the particle properties to the flow behavior of the powder, measured with a powder shear tester under different temperatures. Moreover, Liu [5] developed a similar model predicting the flow behavior of powders from the force balance at the individual particles level. The model provides a good prediction of the flowability measured with a powder shear tester although it has only been tested for one single powder. Finally, Capece [6] established a correlation (see equation (1)) between the flow function coefficient ff_c , measured with shear tests, and a dimensionless population dependent granular Bond number (PGB) Bo_G that depends on the particle properties such as the particles' surface energy, surface roughness, true density and particle size distribution. This model has been established and tested experimentally for powders commonly used in the pharmaceutical industry.

$$ff_c = \alpha \cdot Bo_G^{-\beta} \quad (1)$$

where α and β are adjustable model parameters.

One of the main advantages of this correlation is that it allows a prediction of the macroscopic flowability of a given powder from simple particle properties that are easily measurable or available in the literature. Moreover, the PGB takes into account the whole particle size distribution of polydispersed powders while most of the previous models used mean or median diameters to represent the particle size. The correlation represented by equation (1) has also been observed experimentally using ceramic powders by Bernard-Granger who attempted to take into account the capillary forces in the PGB calculations [7]. Finally, Giraud also extended the model to other powders and showed that the empirical equation (1) was actually consistent with Rumpf's theory [8]. In particular, the exponent parameter β seems to be material independent and comes from the Rumpf's theory, while the proportionality factor α may vary with the consolidation state of the powder bed investigated. According to this last study, equation (2) describes the flow behavior of aluminum, zirconium and yttrium oxide powders with a total squared error of $S^2 = 3.6$ between the experimental data and the model.

$$ff_c = 89.5 \times Bo_G^{-0.54} \quad (2)$$

The PGB, Bo_G , is defined by equation (3), **Error! Reference source not found.** where the size classes of the particle size distribution are indexed from 1 to M, $d_{k,l}$ is the center diameter of the classes k and l , and f_s represents the surface distribution function derived from the volume distribution, assuming that the particles are spherical. Finally, $Bo_{g,kl}$ is the individual granular Bond number (GB), corresponding to the ratio between the interparticle attractive forces and the weight of particles of diameters d_k and d_l , described later in this work. Then, a high PGB value reflects strong cohesive phenomenon within the powder bed, which are likely to reduce its flowability.

$$Bo_G = \left(\sum_{k=1}^M \sum_{l=1}^M \frac{f_s(d_k) \cdot f_s(d_l)}{Bo_{g,kl}} \right)^{-1} \quad (3)$$

However, in most industries handling powders, the granular materials processed are actually multi-component mixtures made of various elementary powders, such as excipients and active ingredients in pharmaceutical compounds. These elementary powders may present various flow behaviors. The amount of each component is then critical for the flowability of the resulting blend. Indeed, it was shown that the flowability of a powder mixture varies significantly depending on its formulation. Actually, it might even exhibit a flow behavior beyond the limits of the flowability of elementary powders [9], [10]. Some studies attempted to predict the flowability of powder mixtures in order to guide industrial R&D labs during formulation development. Most models presented in the scientific literature are black boxes models linking the flowability of powder mixtures to the flowability [11] or the particle characteristics [12] of its elementary powders. These models generally consist in cubic equations whose parameters are fitted by a least square method. Although such an approach gives valuable information on the relative influence of each parameter on the flowability, it only applies to the powders investigated or to powders that share the same physical and chemical properties.

In order to predict the flowability of powder mixtures as a function of their composition, Capece extended the concept of GB and PGB to multi-component mixtures. Then, the multi-component population dependent granular Bond number (MPGB) is defined similarly to the PGB by equation (4), where the number of constituents of the powder mixture are indexed from 1 to N and the size classes of the particle size distributions are indexed from 1 to M [6].

$$Bo_{G,mix} = \left(\sum_{i=1}^N \sum_{j=1}^N \sum_{k=1}^M \sum_{l=1}^M \frac{\omega_{ik} \cdot \omega_{jl}}{Bo_{g,ijkl}} \right)^{-1} \quad (4)$$

In the above equation, ω_{ik} (resp. ω_{jl}) is the ponderation coefficient attributed to the particles of diameter d_k (resp. d_l) belonging to powder i (resp. powder j). ω_{ik} can be computed according to equation (5) from the surface particle size distribution, $f_{,i}$, of powder i and the surface fraction of powder i within the blend, denoted z_i . This means that the model considers a perfect powder mixture, assuming that the contact distribution of a given particle is directly related to the composition of the blend. For example, in a binary mixture containing 50% of particles A and 50% of particles B, we

assume that a given particle is in contact with other particles A or B evenly, whatever the size and shape of these particles.

$$\omega_{ik} = z_i \cdot f_{,i}(d_k) \quad (5)$$

where z_i is deduced from the mass fraction of powder i (resp. j) within the blend, w_i (resp. w_j), using equation (6), which involves the true density of the particles $\rho_{,i}$ (resp. $\rho_{,j}$) and the mean diameter of the surface particle size distribution, $d_{,i}$ (resp. $d_{,j}$).

$$z_i = \left[1 + \sum_{j \neq i}^N \left(\frac{\rho_{,i} d_{,i}}{\rho_{,j} d_{,j}} \cdot \frac{w_i}{w_j} \right) \right]^{-1} \quad (6)$$

The term, $Bo_{g,ikjl}$ of equation (4) is given by equation (7) and corresponds to the individual GB between a particle of powder i of diameter d_k (denoted A on Figure 1) and a particle of powder j of diameter d_l (denoted B on Figure 1).

$$Bo_{g,ikjl} = \frac{F_{ikjl}}{W_{ikjl}} \quad (7)$$

where W_{ikjl} is the geometric mean of the weight of particles A and B, given by equation (8), and F_{ikjl} is the attractive interparticle forces between particles A and B. If the capillary and electrostatic forces are neglected, the Van der Waals force $F_{vdw,ijkl}$ becomes the only relevant interparticle contribution and equation (7) can be modified with $F_{ikjl} = F_{vdw,ijkl}$. In, this paper, the modified Rumpf equation (9) was used for Van der Waals force calculations because of its simplicity and accuracy as compared to experimental results [13].

$$W_{ikjl} = \frac{\pi}{6} g \sqrt{\rho_{,i} \rho_{,j} d_k^3 d_l^3} \quad (8)$$

where g is the gravity constant and $\rho_{,i}$ (resp. $\rho_{,j}$) is the true density of the powder i (resp. j).

$$F_{vdw,ijkl} = \frac{\sqrt{A_i A_j}}{12z_0^2} \left(\frac{\hat{d}_{kl}}{2 \left(1 + \frac{\hat{d}_{asp,ij}}{2z_0} \right)^2} + \frac{3\hat{d}_{asp,ij}\hat{d}_{kl}}{\hat{d}_{asp,ij} + \hat{d}_{kl}} \right) \quad (9)$$

In the above equation, $A_{i,j}$ is the Hamaker constant of the particles constituting the powders i and j , $z_0 = 0.4 \text{ nm}$ is the interparticle distance [14], \hat{d}_{kl} is the harmonic mean of the diameters d_k and d_l and $\hat{d}_{asp,ij}$ is the harmonic mean of the size of the asperities present at the surface of the particles constituting the powders i and j .

This multi-component dimensionless Bond number was shown to correlate well with the flow function coefficient measurements, according to equation (1), for mixtures composed of pharmaceutical powders [6] and ceramic oxide powders [7] even if the α and β empirical parameters of the correlation varies among the authors. However, these differences could be explained by the density of the powders investigated and also by the flow function coefficient measurement protocol [8]. However, despite its efficiency for predicting the flowability of pharmaceutical powder mixtures according to their composition [6], the model still needs to be confirmed with other powder mixtures. Moreover, considering its efficiency, the model could be further extended to other process unit operations handling granular material, such as the grinding process.

In this study, we will extend and confirm the model equation (1) using binary and ternary mixtures of oxide powders exhibiting true densities in a range of 4 to 6 $\text{g}\cdot\text{cm}^{-3}$, quite far from the true densities of pharmaceutical powders tested in previous studies. Various alumina, zirconia and yttrium oxide powders were tested, thus, the results can be compared directly through equation (2) which was found with the same powders [8]. The powder mixtures were prepared thanks to different mixing techniques: a Turbula® mixer (WAB, Sausheim, France) and a ball mill. The Turbula® mixer is a drum rotating through a complex motion that is supposed to ensure a good and quick homogenization of the powder blend [15]. The ball mill consists in a horizontal rotating drum in which pebbles are the grinding media. In such an equipment, a reduction of the particle size takes place simultaneously with the mixing operation. This allows homogenization at a much finer scale [16]. Indeed, not only smaller

particle size increases the number of particles, leading to finer potential homogeneity [17], but the grinding pebbles also acts as mixing aids, acting positively on the kinetics of the diffusion mixing mechanism [18]. The aim of this paper is to predict the flowability of oxide powder mixtures prepared in a Turbula® mixer and in a ball mill according to their composition and from the particle properties of the elementary bulk powders the blends are made of.

2. Materials and Methods

2.1. Powders

Five different ceramic oxide powders have been studied. They all exhibit different flow behaviors, from free flowing to very poor flowability, and different particle properties, such as particle size distributions, particle surface roughness, surface energy and true density. The powders investigated are listed below:

- Two different grades of alumina powders: GE15 and CR6 (Baikowski®, Poisy, France).
- Two different grades of zirconia powders: GY3Z-R60 and CY3Z-RA (Saint Gobain®, Courbevoie, France).
- An yttrium oxide powder: grade C (H.C. Starck®, Newton, USA).

In this paper, alumina GE15, alumina CR6, zirconia GY3R-R60, zirconia CR3Z-RA and yttria grade C are referred to as Al_2O_3 G, Al_2O_3 C, ZrO_2 G, ZrO_2 C and Y_2O_3 C respectively.

2.2. Characterization methods

All the powders investigated were characterized in terms of flowability, particle size distribution, true density and surface energy. The PGB of single powders were computed from these characterization results for all the powders, according to the methodology described previously for $N = 1$.

2.2.1. Powder flowability

Before any rheological measurement, all the samples were dried in a stove at 110 °C for 24 h in order to remove the residual moisture content of the powders that may induce capillary forces between the particles under ambient conditions (23°C and 40% relative humidity). Shear testing were performed with a FT4® powder rheometer (Freeman, Tewkesbury, UK) in a 10 mL cylindrical cell. After

conditioning and pre-consolidation steps of the powder bed under a normal stress of 9 kPa, shear tests were performed successively under 3, 4, 5, 6 and 7 kPa normal stresses following the Jenike standard procedure [19]. According to Mohr-Coulomb's theory, the yield locus points (see figure 2), obtained by shearing the powder under different normal stresses, are expected to be aligned in the Mohr's space, thus forming the following yield locus line :

$$\tau = \mu\sigma + c \quad (10)$$

where τ and σ represent the shear and normal stresses respectively, c is the cohesion of the powder, and μ is the friction coefficient which is related to the angle of internal friction φ by equation (11).

$$\mu = \tan \varphi \quad (11)$$

The cohesion of the powder represents its natural resistance to flowability under no normal stress application; it originates from the interparticle forces. On the other hand, the friction coefficient comes from the mechanical friction that occurs between the surfaces of the particles in contact.

The Mohr circles of Figure 2 are constructed geometrically from the yield locus line: the small Mohr circle is tangent to the yield locus and passes through the origin while the large Mohr circle is also tangent to the yield locus but passes through the pre-consolidation point, denoted by C on Figure 2. The cohesion stress f_c and the major consolidation stress σ_1 correspond to the shear stress values of the highest intersection between the x-axis and the small and large Mohr circles, respectively. Finally, the flow function coefficient ff_c corresponds to the ratio between the major consolidation stress and the cohesion stress, as shown in equation (12).

$$ff_c = \frac{\sigma_1}{f_c} \quad (12)$$

The classification given in Table 1 is often used in order to assess and rank the flow behavior of a given powder [20]. The flow function coefficient is expected to vary with the pre-consolidation stress, meaning that the flowability may vary according to the mechanical stress applied to the powder bed.

The flow function coefficient ff_c , the cohesion c and the angle of internal friction of the powders investigated are reported in Table 2. Each measurement was carried out twice. The values in the table correspond to the average of both measurement and the uncertainty corresponds to the standard deviation. Concerning the ZrO₂ G powder, the cohesion measured was slightly below zero, meaning that this powder exhibits a free flowing behavior under that level of consolidation. Thus, its cohesion was kept to 0 kPa and the flow function coefficient was not computed. According to Table 1, the Al₂O₃ C and the Y₂O₃ C powders seem to exhibit very poor flowability, while the Al₂O₃ G powder flows easily and the ZrO₂ C and ZrO₂ G powders are free flowing. However, it should be noted that the flowability of the ZrO₂ C powder is smaller than that of the ZrO₂ G powder despite the fact that they belong to the same flowability grade according to Table 1.

2.2.2. True density

The true density ρ of the particles constituting the powders investigated were measured with a helium pycnometer AccuPyc II 1340® (Micromeritics, Mérignac, France) in a 10 mL cell. Five samples were considered for each powder, the average value being retained. The uncertainty intervals were calculated through the standard deviation. For each sample, between three and six cycles of measurements were performed at 23 °C and 19.6 PSI (135 kPa). Each cycle includes 25 purges followed by 25 measurements. The true densities of the powders are given in Table 3.

2.2.3. Particle size distribution

The particle size distributions of the powders were measured by LASER diffraction with a Mastersizer 3000® (Malvern, Malvern, UK) which gives the particle size distribution through $M = 100$ size classes. The liquid dispersion unit (Hydro MV®) was employed in order to avoid re-agglomeration that may occur during dry dispersion. The Mie theory was used for the particle diameters calculations. Ten samples were measured per powder and each sample was measured ten times after a defined immersion time inside the liquid dispersion unit. The average particle size distribution was kept for each powder and the uncertainty intervals are given by the standard deviations. The particle size distributions in volume fraction are given on Figure 3. They may be converted in surface fraction by assuming that particles are spherical. It appears that the powders containing the smallest particles are

those exhibiting the worst flowability (see Table 2). The Sauter mean diameters corresponding to each powder is also given in Table 3.

2.2.4. Particle surface energy

The Hamaker constants A of the powders were calculated from the Frenkel equation (13) [14], where $D_0 \approx 0.165 \text{ nm}$ is a cut-off distance and γ^d is the dispersive surface energy of the particles.

$$A = 24\pi D_0^2 \gamma^d \quad (13)$$

The dispersive surface energy is measured by dynamic vapor sorption DVS (SMS, London, UK) from the sorption isotherm of heptane at 25 °C, using the Fowkes model [21]. This method was shown to give results that are accurate and similar to those obtained by inverse gas chromatography for alumina powders [22]. The Hamaker constant values are given in Table 3.

2.3. Population dependent granular Bond number of the bulk powders

In this study, the Van der Waals forces are the only interparticle forces considered. Indeed, electrostatic forces were neglected after measuring the electrostatic charge developed by the powders using a tribo-electrification technique. Capillary forces are also neglected since all the samples are dried in a stove before flowability measurements. The PGB is then computed from the particles properties using equation (3). The Rumpf's modified equation (7) is used for the Van der Waals forces calculation, in which the asperity diameter is assumed to be $d_{as} = 200 \text{ nm}$ for each powder. This assumption is consistent with AFM measurements carried out in contact mode with a confocal Raman microscope alpha300R (WITec®, Ulm, Germany). More details concerning the PGB calculation for the raw powders are available in [8]. The corresponding PGB values are given in Table 3.

2.4. Preparation of the powder mixtures

2.4.1. Preparations in a Turbula® mixer

The powder mixtures were prepared in a Turbula® T2F mixer (WAB, Sausheim, France) for 10 minutes, at a rotational speed of 32 rpm, which are standard conditions to ensure a good homogeneity of the mixtures [15]. Furthermore, a complementary study, focusing on the homogeneity of such mixtures has been carried out by analyzing the composition of various 2 mL samples, randomly taken

from the blends. The composition of the samples could be measured from helium pycnometry tests, knowing that zirconia and alumina have significantly different true densities (see section 2.2.2). The results showed that the variation of composition over a large amount of samples was not significant (variation coefficient below 3% after ten samples), allowing to conclude that the blends must be homogeneous at the scale of FT4® measurements (10 mL cells). The blends were prepared in a 300 mL polyethylene vessel, filled at a filling ratio of 40% in volume and fixed inside the 2 L Turbula® vessel.

2.4.2. Preparations using a ball mill

In order to compare different mixing techniques and to investigate the effect of particle size reduction on the flowability, some binary mixtures containing ZrO₂ C and Al₂O₃ G powders have been prepared in a ball mill. The mill is made of a 1 L cylindrical INOX vessel filled with 500 cylindrical 8x8 mm steel pebbles, which are used as grinding media and mixing aids. The amount of pebbles and powder incorporated is defined in order to get a filling ratio and a powder level of $J = 0.3$ and $U = 1.00$ respectively. J and U are defined by equations (14) and (15) respectively. Such filling conditions correspond to optimal operating conditions of a ball mill [18], [23].

$$J = \frac{\text{Volume of the pebbles bed}}{\text{Volume of the vessel}} \quad (14)$$

and,

$$U = \frac{\text{Volume of the powder bed}}{\varepsilon_g \cdot \text{Volume of the pebbles bed}} \quad (15)$$

where ε_g is the porosity of the pebbles bed, which was observed to be around $\varepsilon_g = 0.33$ by measuring the height of the pebble bed filled in a transparent vessel of approximately the same size and shape than the milling vessel.

The vessel, filled with the powders and the pebbles, is rotating horizontally at 25 rpm around its longitudinal axis. The rotational speed is chosen in order to get a Froude number Fr, defined in

equation (16), equal to 0.04, so as to ensure a cascade motion regime of the pebbles inside the vessel [24].

$$Fr = \frac{\omega^2 D}{2g} \quad (16)$$

where ω is the angular rotational speed and D corresponds to the vessel diameter.

The cascade motion regime, represented on Figure 4, is obtained when the rotational speed is sufficient to eject some pebbles from the pebble bed, but not too high in order to ensure that the impact point of the dropping pebbles is located on the pebble's bed, and not on the walls of the vessel [24], [25]. This motion regime is suitable for both mixing, combining convection and diffusion mixing mechanisms, and size reduction of the particles, combining impact, compression and shear fragmentation mechanisms [26].

3. Experimental results and discussion

3.1. Validity of the power law parameters

Before comparing the experimental results to the predictive power law represented by equation (2), we must make sure of its validity. Indeed, equation (2) not only comes from the Rumpf theory, which actually gives a link between the granular Bond number and the cohesion, but also depends on the relation linking the flow function coefficient to the cohesion, both being measured during the shear tests. Actually, Giraud previously found a power law relation given by equation (17) between the flow function coefficient and the cohesion, leading to the exponent $\beta = 0.54$ in equation (2) [8].

$$ff_c \approx 4.66 \times c^{-0.90} \quad (17)$$

Thus, such correlation has been made up using all the powder samples analyzed in this study; this includes the raw powders, the powder mixtures and the milled and co-milled powders. The relation (18) has been found, whose coefficients are close enough to equation (17). This is not surprising since the powder used in this study are the same than those tested to obtain equation (17).

$$ff_c \approx 4.65 \times c^{-0.92} \quad (18)$$

Therefore, the exponent $\beta = 0.54$ can be considered in the model equation (1) to make predictions for both the mixed and ground powders prepared in this study.

3.2. Predicting the flowability of the powder mixtures

Various binary and ternary mixtures have been prepared using the powders described in section 2.1 for different compositions. The mixing conditions are detailed in section 2.4.1. The blends are summarized in Table 4, some of them being carried out twice in order to check the repeatability of the mixing operation. The flowability of each blend was then characterized with the FT4® rheometer using exactly the same conditions than for the raw powders, described in section 2.2.1. This includes drying the blends in a stove at 110 °C for 24 h before the measurements. At least two samples were characterized per blend, the average being kept and the standard deviation being used as an uncertainty interval.

The flow function coefficient and the cohesion of each blend are given in Table 4. Then, the evolution of the flow function coefficient along with the composition of some binary mixtures is plotted on Figure 5. The mass fraction of the worst flowing powder is represented on the x-axis. The crosses correspond to the experimental results given in Table 4. It is interesting to note that for all the examples in Figure 5, the flowability of the mixtures seems to be mostly influenced by the worst flowing powder. Indeed, a small fraction of a poorly flowing powder seems to affect significantly the flowability of the whole blend, while a small fraction of an easily flowing powder does not improve the flowability of the blend. It holds also true for the ternary mixtures made of ZrO₂ C, Al₂O₃ G and Y₂O₃ C powders, whose flow function coefficients are given in Table 4: the ternary mixture containing approximately one third of each component almost exhibits a very poor flowability despite the fact that the Al₂O₂ G and ZrO₂ C compounds exhibit respectively easy and free flowing behaviors. These observations are consistent with the Hamaker theory, which states that the Van der Waals force acting between two spherical particles is mainly fixed by the size of the smallest, and thus, worst flowing particle [27].

Since all five elementary powders under investigation have been fully characterized (Table 3 and Figure 3), the MPGB related to all the corresponding mixtures were computed using the methodology presented in section 1. Indeed, the MPGB can be computed for any mixture knowing its composition and the properties of its raw constituting powders. Thus, the flow function coefficient of the mixtures is plotted on Figure 6 as a function of the MPGB. The black dots on Figure 6 corresponds to the raw powders and the model established for these single powders, described by equation (2) ($\alpha = 89.5$ and $\beta = 0.54$), is represented by the dotted line. All the other points of this graph correspond to various binary and ternary mixtures of Table 4 prepared and characterized for this study. Finally, the continuous line corresponds to the correlation given by equation (1) where the exponent $\beta = 0.54$ comes from the Rumpf's theory, and the proportionality factor $\alpha = 82.7$ is adjusted with a least square method in order to fit the experimental data, with a total squared error of $S^2_{mix} = 41.9$. This error has to be compared with the total squared error obtained for the model (2) established for single powders: $S^2_{ingle} = 3.6$. Although the error corresponding to the model established with powder mixtures is higher, we can conclude that it is still relevant, considering the fact that much more experimental data have been recorded. It should also be noted that the total squared error computed is strongly influenced by the presence of the mixture containing the Al_2O_3 G and the ZrO_2 C powders, which seems to behave differently, when compared to the other powder mixtures according to Figure 6. Indeed, the total squared error falls to $S'^2_{mix} = 22.4$ when the contribution of the Al_2O_3 G / ZrO_2 C mixture is removed. An explanation for the behavior of this particular mixture is provided later. The correlation obtained for mixtures of powders is then given by equation (19).

$$ff_c = 82.7 * B_{O_G,mix}^{-0.54} \quad (19)$$

We can notice on Figure 6 that the correlation obtained for powder mixtures is very close to that found for the raw powders only. Indeed, the proportionality factor found for the raw powder ($\alpha = 89.5$ in equation (2)) is close to that obtained when the powder mixtures are added for completing the fit ($\alpha = 82.7$ in equation (19)). Thus, we can conclude that the correlation also applies to powder mixtures, as suggested previously by Capece [6]. Accordingly, it can be employed as a predictive model to assess the flow function coefficient of powder mixtures according to their formulation and

raw powders characteristics. Moreover, we can notice that the ternary mixtures, represented by the triangles on Figure 6, seem to behave according to the same power law (equation (19)) than the binary mixtures. This suggests that the model applies to multi-component mixtures. However, this should be completed by more experimental data in future studies.

The value of the MPGB was computed for all the mixtures investigated using the raw powders properties. Then, equation (19) is employed to predict the flow function of all the blends. The evolution of the flow function coefficient predicted by the model is represented by the dotted lines on Figure 5, for a confidence interval of 90% along with the experimental data represented by the crosses. For all mixtures, the model predictions are in good agreement with the empirical results. The blend for which the predictions are the less accurate is the mixture containing ZrO_2 C and Al_2O_3 G powders, both raw powders exhibiting very similar flowability. This may be explained by the fact that those powders share a similar particle size as suggested by their Sauter mean diameters provided in Table 3. Thus, we can assume that the flowability of such a mixture is mostly governed by secondary factors, which are not taken into account in this model such as the particle shape or the packing structure. However, the predictions are very accurate for mixtures involving powders exhibiting various flow behaviors and can be used to guide industrial manufacturers for the formulation of their powder mixtures. In particular, the model seems to predict accurately the fact that the flowability of the whole mixture is driven by the flowability of the worst flowing raw powder. Indeed, a sensitivity analysis of the PGB carried out in a previous study [8] showed that the amount of fine particles among the particle size distribution is a first order parameter, having a great influence on the value of the granular Bond number. Then, adding a small amount of fine particles to a powder mixture will have a significant detrimental impact on the value of the Bond number, and then, on the predicted flow function coefficient.

As an example of application, the model predicts a flow function coefficient of 6 (easy flowing in Table 1) for powder mixtures containing ZrO_2 C and Al_2O_3 C powders for a mass content of alumina of 10%. The model also predicts that changing the alumina content of this mixture from 10% to 20% would decrease the flow function coefficient under 4, leading then to a poor flowability. However, it is

still possible to get an easy flowing zirconia and alumina powder mixture containing 20% of alumina by replacing the ZrO_2 C powder by ZrO_2 G in the mixture. Indeed, the predicted flow function coefficient of the mixture containing 80% of ZrO_2 G and 20% of Al_2O_3 C is approximately 5, corresponding to an easy flow behavior.

3.3. Application of the model for milled and co-milled powders

In order to investigate the kinetics of size reduction during the ball mill operation, three different milling conditions were tested for the following milling times: 1, 4 and 8 minutes. These correspond respectively to 25, 100 and 200 full revolutions of the drum. These operating conditions are summarized in Table 5 and referred to as B01, B02 and B03 respectively. Otherwise, all millings were performed at the same rotational speed and with the same powder/pebbles filling ratios, as described in section 2.4.2. Milling was first performed with the raw Al_2O_3 G and ZrO_2 C powders only, and then for binary mixtures of these two powders containing 30% mass fraction of Al_2O_3 G. Another blend containing 50% of each powder has also been milled but only in the B02 condition. In each case, the powders have been introduced as layers in the drum, starting with the worst flowing powder, without any pre-mixing step. As for mixture preparations, a complementary study focusing on the homogeneity of these co-millings has been carried out following the same procedure used for Turbula® preparations, described in section 2.4.1. The results were roughly the same, showing that the mixtures obtained by co-milling in these conditions were homogeneous at a much finer scale than the FT4® 10 mL cell.

After milling, the flowability of the collected powders were characterized using the FT4® powder shear tester with the same analyzing conditions than those described in section 2.2.1 for the raw powders. The results are given in Table 5. As expected, the flowability of the powders decreases with the milling time. It can be noted that the flowability of the ZrO_2 C powder becomes worse than that of the Al_2O_3 G powder after milling under the same conditions. This could be due to the fact that ZrO_2 C particles seem quite spherical as compared to other powders and become more angular after milling, while Al_2O_3 G particles are already non spherical and irregular before milling, as shown on Figure 7. Then, one can expect the flowability of ZrO_2 C powder to be more sensible to milling. Regarding the

co-milled powders, the value of their flow function coefficient is always between the values of the flow function coefficients of the raw powders milled under the same conditions. In addition, for the co-milled powders using the B02 condition listed in Table 5, the mixture containing 70% of ZrO_2 C powder, which is the worst flowing compound after milling, exhibits a lower flowability than the mixture containing 50% of ZrO_2 C.

The particle size distribution of the powders after milling and co-milling have also been measured by LASER diffraction. The measurements conditions are the same than those described in section 2.2.3 for the raw powders. The particle size distribution of the ZrO_2 C and Al_2O_3 G powders after milling under conditions B01, B02 and B03 are represented on Figure 8 and Figure 9 respectively. As expected, the amount of fine particles increases with the milling time. We can also notice that the ZrO_2 C powder seems to be more sensitive to milling than the Al_2O_3 G powder. That could explain why the flowability of the ZrO_2 C powder becomes worse than that of the Al_2O_3 G powder after milling under the same conditions. DVS and helium pycnometry measurements have also been carried out for some milled powders. It resulted in the fact that the Hamaker constant and the true densities of the powders remained identical, whatever the milling conditions. We also assumed that the particle asperities size was still approximately $d_{as} = 200 \text{ nm}$ in all cases. Then, the PGB of the milled Al_2O_3 G and ZrO_2 C powders have been computed from their particle sizes, using the Hamaker constants, true densities and surface asperity diameters of the raw powders. The MPGB of the co-milled powders have also been computed from the properties of the elementary powders milled under the same conditions. For example, the MPGB of the co-milled powder containing 70% of ZrO_2 C and 30% of Al_2O_3 G using the B03 condition is computed from the properties of the ZrO_2 C and Al_2O_3 G raw powders milled under the same condition. Thereby, we assume that the flowability of the co-milled powder is the same as the flowability of the mixture containing both pre-milled powders.

The flow function coefficients of the milled and co-milled powders are then plotted as a function of the PGB, for milled powders, and of the MPGB, for co-milled powders (see Figure 10). Black dots correspond to the bulk powders and the correlation (19) obtained in section 3.2 for powder mixtures is represented by the continuous line. The experimental data corresponding to milled powders (triangles

for milled Al₂O₃ G powder and squares for milled ZrO₂ C powder) and co-milled powders (crosses) are situated on the same power law, as stated in equation (1). In this case, the coefficients of the power law are $\beta = 0.54$, given by the Rumpf theory, and $\alpha = 179.6$ fitted in order to match the experimental data using a least squares method with a squared error of $S^2_{mill} = 1.7$. This value may be compared with the total squared error obtained for the model represented by equation (2) established for single raw powders: $S^2_{ingle} = 3.6$. The correlation represented by equation (20), obtained with milled and co-milled powders is not exactly the same than that obtained for raw powders although they are quite close.

$$ff_c = 179.6 * B_{O_{G,mix}}^{-0.54} \quad (20)$$

The difference can be explained by the fact that the powder bed structure changes after milling the powders. Indeed, it was shown that the proportionality factor α may vary with the powder bed porosity and coordination number. Moreover, the model parameters might also be affected by the value of the asperity size diameter, which has been kept constant at $d_{asp} = 200 \text{ nm}$ while this might be no longer true after milling the powders.

The evolution of the flow function coefficient of the co-milled ZrO₂ C and Al₂O₃ G powders is plotted as a function of the alumina mass fraction on Figure 11 for the different milling conditions investigated. The crosses correspond to the experimental measurements presented in Table 5 and the dotted lines correspond to the model predictions based on the MPGB calculations and equation (20) for a confidence interval of 90%. Unlike for powder mixtures, presented on Figure 5, the flow function coefficient increases when the mass fraction of alumina powder increases. This is because the ZrO₂ C powder becomes the worst flowing compound after milling. According to this Figure 11, the model predictions seem to be in good agreement with the experimental data for each co-milled powders formulations. However, they seem to be a bit less accurate for a powder containing very small particles such as the ZrO₂ C powder milled in B03 conditions. Indeed, this powder media exhibits a large amount of fine particles, as shown on Figure 8, giving a very high MPGB that in turn gives rise to a predicted flow function coefficient of 0.57 according the model equation (20). For comparison,

the flow function coefficient measured is actually 1.29. One possible explanation is that such small particles may re-agglomerate easily together to form bigger particles, making the measured particle size distribution not representative of the size of the particles during flow measurements. Then, some care should be taken when exploiting such results because the calculated MPGB value is very sensitive to the amount of fine particles. Moreover, the shear testing method is not the most accurate when dealing with very poor flowing powders for which the flow function coefficient is under 1.5. In this case, other flow measurement techniques, allowing smaller pre-consolidation stresses, such as the Schultz ring tester [9], might provide more accurate and relevant results.

4. Conclusion and perspectives

As a conclusion, the model described by equation (1) gives a link between the microscopic properties of the particles and the macroscopic flow behavior of powders, as suggested in the literature. In this paper, we have shown that this model can also be employed to predict the evolution of the flowability of powder mixtures according to their composition, given the particle properties of the raw powders. The multi-component population dependent granular Bond number has been used successfully to represent the force balance at the particle level within the mixture. It also takes into account the polydispersity of each powder constituting the blend. Thus, the model predictions represented by equation (19) are in good agreement with the experimental results obtained by preparing binary and ternary mixtures in a Turbula® mixer. This allows us to anticipate the flow function coefficient of a powder mixture for a given composition. Therefore, this model may be used to quickly estimate the influence of a variation of the composition of a given powder mixture on its flowability. For example, it is possible to assess which range of product formulations are compatible with the conveying and storage equipment implemented in a given process.

Moreover, the macro-micro link represented by equation (1) was also shown to be accurate for powders ground in a ball mill for different milling conditions. However, the proportionality factor α obtained in equation (20) was slightly different from that obtained in equation (19) for raw and mixed powders. This may be due to the fact that this proportionality factor depends on the powder bed packing structure, which is likely to change after milling. Nonetheless, the evolution of the flowability

of the powders according to their size reduction during ball milling was shown to follow accurately the model predictions. Then, the evolution of the flowability of powders according to the milling time can be predicted through equation (20) if the evolution of the size reduction according to the milling time is known, through a population balance approach for example [28]. This can help to define the optimal residence time in a continuous or discontinuous mill by taking into account the evolution of the flow behavior of the milled powder. Moreover, the model also may be used in reverse, to get an idea of the particle size distribution, or at least its population-dependent granular Bond number, after grinding thanks to a simple shear test. Such reverse correlation, allowing estimating the particle size distribution from flowability tests, should be further explored in future works.

Furthermore, it was shown that equation (20) was also consistent with the properties of co-milled powders for various blend compositions and different milling conditions. The flowability of a co-milled powder can then be predicted through this model by using the multi-component population dependent granular Bond number, computed from the particle properties of the raw powders milled in the same conditions. This suggests that a co-milled powder behaves like a powder mixture of the same powders milled in the same conditions.

Despite its strong ability to predict the flowability of powder mixtures, milled and co-milled powders, this model can still be improved by a better knowledge of the elementary particles properties. In particular, the powder bed packing structure [29], especially for powder mixtures, the asperity diameter at the surface of an individual particle, and the particle shape [30] should be further investigated and taken into account in the Bond number calculations.

Bibliography

- [1] J. P. K. Seville, C. D. Willett, and P. C. Knight, “Interparticle forces in fluidisation: a review,” *Neptis Symp. Fluid.- Present Future*, vol. 113, no. 3, pp. 261–268, Dec. 2000, doi: 10.1016/S0032-5910(00)00309-0.
- [2] M. E. Aulton, *Pharmaceutics : the science of dosage form design*. Edinburgh; New York: Churchill Livingstone, 2002.
- [3] Q. Li, V. Rudolph, B. Weigl, and A. Earl, “Interparticle van der Waals force in powder flowability and compactibility,” *Int. J. Pharm.*, vol. 280, no. 1, pp. 77–93, Aug. 2004, doi: 10.1016/j.ijpharm.2004.05.001.
- [4] I. Tomasetta, D. Barletta, and M. Poletto, “Correlation of powder flow properties to interparticle interactions at ambient and high temperatures,” *Particuology*, vol. 12, pp. 90–99, 2014, doi:10.1016/j.partic.2013.02.002.
- [5] L. X. Liu, I. Marziano, A. C. Bentham, J. D. Litster, E.T.White, and T. Howes, “Effect of particle properties on the flowability of ibuprofen powders,” *Int. J. Pharm.*, vol. 362, no. 1, pp. 109–117, Oct. 2008, doi: 10.1016/j.ijpharm.2008.06.023.
- [6] M. Capece, K. R. Silva, D. Sunkara, J. Strong, and P. Gao, “On the relationship of inter-particle cohesiveness and bulk powder behavior: Flowability of pharmaceutical powders,” *Int. J. Pharm.*, vol. 511, no. 1, pp. 178–189, Sep. 2016, doi: 10.1016/j.ijpharm.2016.06.059.
- [7] G. Bernard-Granger, M. Giraud, E. Pascal, L. Mailhan, T. Larsson, C. Valot, C. Ablitzer, C. Gatumel, and H. Berthiaux, “Rheological properties of alumina powder mixtures investigated using shear tests,” *Powder Technol.*, vol. 345, pp. 300–310, 2019, doi:10.1016/j.powtec.2019.01.027.
- [8] M. Giraud, C. Gatumel, S. Vaudez, G. Bernard-Granger, J. Nos, T. Gervais, and H. Berthiaux, “Investigation of a granular Bond number based rheological model for polydispersed particulate systems,” *Chem. Eng. Sci.*, p. 115971, 2020, doi:10.1016/j.ces.2020.115971.

- [9] A. Vasilenko, B. J. Glasser, and F. J. Muzzio, "Shear and flow behavior of pharmaceutical blends — Method comparison study," *Powder Technol.*, vol. 208, no. 3, pp. 628–636, Apr. 2011, doi: 10.1016/j.powtec.2010.12.031.
- [10] N. Vlachos and I. T. H. Chang, "Investigation of flow properties of metal powders from narrow particle size distribution to polydisperse mixtures through an improved Hall-flowmeter," *Powder Technol.*, vol. 205, no. 1, pp. 71–80, 2011, doi:10.1016/j.powtec.2010.08.067.
- [11] Y. Wang, R. D. Snee, W. Meng, and F. J. Muzzio, "Predicting flow behavior of pharmaceutical blends using shear cell methodology: A quality by design approach," *Powder Technol.*, vol. 294, pp. 22–29, 2016, doi:10.1016/j.powtec.2016.01.019.
- [12] W. Yu, K. Muteki, L. Zhang, and G. Kim, "Prediction of Bulk Powder Flow Performance Using Comprehensive Particle Size and Particle Shape Distributions," *J. Pharm. Sci.*, vol. 100, no. 1, pp. 284–293, 2010, doi: 10.1002/jps.22254.
- [13] Y. Chen, J. Yang, R. N. Dave, and R. Pfeffer, *Fluidization of coated group C powders*, vol. 54, no. 1. 2008.
- [14] J. N. Israelachvili, "Chapter 13 - Van der Waals Forces between Particles and Surfaces," in *Intermolecular and Surface Forces (Third Edition)*, San Diego: Academic Press, 2011, pp. 253–289.
- [15] C. Mayer-Laigle, C. Gatumel, and H. Berthiaux, "Mixing dynamics for easy flowing powders in a lab scale Turbula® mixer," *Chem. Eng. Res. Des.*, vol. 95, pp. 248–261, Mar. 2015, doi: 10.1016/j.cherd.2014.11.003.
- [16] P. K. Chaudhuri and D. W. Fuerstenau, "The effect of mixing aids on the kinetics of mixing in a rotating drum," *Powder Technol.*, vol. 4, no. 3, pp. 146–150, Mar. 1971, doi: 10.1016/0032-5910(71)80023-2.
- [17] P. M. C. Lacey, "Developments in the theory of particle mixing," *J. Appl. Chem.*, vol. 4, no. 5, pp. 257–268, 1954, doi: 10.1002/jctb.5010040504.
- [18] K. Shoji, L. G. Austin, F. Smaila, K. Brame, and P. T. Luckie, "Further studies of ball and powder filling effects in ball milling," *Powder Technol.*, vol. 31, no. 1, pp. 121–126, 1982, doi:10.1016/0032-5910(82)80013-2.

- [19] EFCE, *Standard shear testing technique for particulate solids using the jenike shear cell*, EFCE Working Party on the Mechanics of Particulate. Institution of Chemical Engineers, 1989.
- [20] M. Leturia, M. Benali, S. Lagarde, I. Ronga, and K. Saleh, “Characterization of flow properties of cohesive powders: A comparative study of traditional and new testing methods,” *Powder Technol.*, vol. 253, pp. 406–423, Feb. 2014, doi: 10.1016/j.powtec.2013.11.045.
- [21] C. L. Levoguer and D. R. Williams, “Measurement of the surface energies of pharmaceutical powders using a novel vapor adsorption method,” Surface Measurement Systems Ltd, UK, Application note 17.
- [22] C. Tisserand, R. Calvet, S. Patry, L. Galet, and J. A. Dodds, “Comparison of two techniques for the surface analysis of alumina (Al₂O₃): Inverse Gas Chromatography at Finite Concentration (IGC-FC) and Dynamic Vapor Sorption (DVS),” *Powder Technol.*, vol. 190, no. 1, pp. 53–58, 2009, doi:10.1016/j.powtec.2008.04.058.
- [23] E. Petrakis, E. Stamboliadis, and K. Komnitsas, “Identification of Optimal Mill Operating Parameters during Grinding of Quartz with the Use of Population Balance Modeling,” *KONA Powder Part. J.*, vol. 34, pp. 213–223, 2017, doi: 10.14356/kona.2017007.
- [24] J. Mellmann, “The transverse motion of solids in rotating cylinders—forms of motion and transition behavior,” *Powder Technol.*, vol. 118, no. 3, pp. 251–270, Aug. 2001, doi: 10.1016/S0032-5910(00)00402-2.
- [25] Hans. Rumpf, *Particle technology*. London: Chapman and Hall, 1990.
- [26] Y. Arai, *Chemistry of Powder Production*. Springer Netherlands, 1996.
- [27] H. C. Hamaker, “The London—van der Waals attraction between spherical particles,” *Physica*, vol. 4, no. 10, pp. 1058–1072, Oct. 1937, doi: 10.1016/S0031-8914(37)80203-7.
- [28] G. Matijašić and A. Glasnovic, “Batch Grinding in Laboratory Ball Mills: Selection Function,” *Chem. Eng. Technol.*, vol. 32, 2009.
- [29] L. Legoix, C. Gatumel, M. Milhé, and H. Berthiaux, “Characterizing powders in order to determine their flow behavior in a mixer: From small scale observations to macroscopic in-mixer rheology for powders of various flowabilities,” *Powder Technol.*, vol. 322, pp. 314–331, Dec. 2017, doi: 10.1016/j.powtec.2017.07.075.

- [30] G. Thomas, Y. Ouabbas, P. Grosseau, M. Baron, A. Chamayou, and L. Galet, “Modeling the mean interaction forces between powder particles. Application to silica gel–magnesium stearate mixtures,” *Appl. Surf. Sci.*, vol. 255, no. 17, pp. 7500–7507, Jun. 2009, doi: 10.1016/j.apsusc.2009.03.099.

List of figures:

Figure 1: Forces applied between two spherical particles A, of nature i and size d_k , and B, of nature j and size d_l , in close contact

Figure 2: Mohr-Coulomb yield locus and Mohr circles

Figure 3: Particle size distribution in volume fraction of the powders investigated, as measured by LASER diffraction with a liquid dispersion unit

Figure 4: Different motion regimes of the pebbles in a ball mill while increasing the rotational speed of the drum

Figure 5: Evolution of the flow function coefficient for binary mixtures. The crosses correspond to FT4® measurements and the dotted lines to model predictions for a confidence interval of 90%

Figure 6: Flow function coefficient, as measured by a FT4® powder rheometer, plotted as a function of the MPGB, computed from the particles properties, for all the elementary powders (dots) and for various binary and ternary powder mixtures

Figure 7: SEM pictures (x800 magnitude) of the Al_2O_3 G (up) and ZrO_2 C (down) powders, before (left) and after milling in B02 conditions (right)

Figure 8: Particle size distribution of the ZrO_2 C powder before and after milling under different conditions (B01, B02 and B03)

Figure 9: Particle size distribution of the Al_2O_3 G powder before and after milling under different conditions (B01, B02 and B03)

Figure 10: Flow function coefficient, as measured by a FT4® rheometer, plotted as a function of the MPGB, computed from the particles properties, for all the elementary powders (dots), various binary and ternary mixtures (plus) and milled (triangles and squares) and co-milled powders (crosses)

Figure 11: Evolution of the flow function coefficient of powders obtained by co-milling according to their composition. The crosses correspond to FT4® measurements and the dotted lines to model predictions for a confidence interval of 90%

List of tables:

Table 1: Classification of the flowability of powders according to their flow function coefficient

Table 2: Flowability of the bulk powders investigated, as measured by a FT4® powder rheometer in a 10 mL cylindrical cell under a 9 kPa pre-consolidation stress

Table 3: Bulk powder properties and population dependent granular Bond number calculated from these properties

Table 4: Flow function coefficient and cohesion of the binary and ternary powder mixtures prepared in a Turbula® mixer

Table 5: Flow function coefficient and cohesion of the milled and co-milled powders obtained in a ball mill

Table 1.

Flow function coefficient	Flowability
$ff_c < 1$	Not flowing
$1 < ff_c < 2$	Very poor
$2 < ff_c < 4$	Poor
$4 < ff_c < 10$	Easy
$ff_c > 10$	Free flowing

Table 2.

Powder	Flow function coefficient ff_c (-)	Cohesion c (kPa)	Friction coefficient μ (-)
ZrO ₂ G	---	0	0.47 ± 0.004
ZrO ₂ C	12.5 ± 1.43	0.34 ± 0.04	0.48 ± 0.011
Al ₂ O ₂ G	8.42 ± 0.11	0.54 ± 0.01	0.68 ± 0.006
Y ₂ O ₃ C	1.58 ± 0.05	3.32 ± 0.14	0.65 ± 0.007
Al ₂ O ₃ C	1.19 ± 0.04	4.57 ± 0.31	0.72 ± 0.003

Table 3.

Powder	True density ρ (g.cm ⁻³)	Sauter mean diameter D (μ m)	Span of the distribution <i>span</i>	Hamaker constant A (10 ⁻¹⁹ J)	Asperity size d_{asp} (nm)	PGB Bo_G (-)
ZrO ₂ G	5.408 ± 0.010	52.6	2.08	1.13 ± 0.08	200	7.40 x 10 ⁰
ZrO ₂ C	5.874 ± 0.012	21.3 ± 11.1	1.04 ± 0.06	1.50	200	(3.39 ± 0.66) x 10 ¹
Al ₂ O ₃ G	4.017 ± 0.070	23.1 ± 1.3	2.07 ± 0.10	1.57 ± 0.03	200	(1.16 ± 0.05) x 10 ²
Y ₂ O ₃ C	4.986 ± 0.093	5.4 ± 3.5	13.6 ± 5.88	1.42	200	(2.57 ± 1.32) x 10 ³
Al ₂ O ₃ C	4.080 ± 0.005	4.4 ± 0.8	4.28 ± 1.20	1.56	200	(1.09 ± 0.23) x 10 ⁴

Table 4.

Elementary powders	Composition	Blend repetition / samples per blend	Flow coefficient ff_c (-)	function ff_c (-)	Cohesion c (kPa)
ZrO ₂ G / Al ₂ O ₃ G	0.90 / 0.10	1 / 2	22.1		0.19
	0.80 / 0.20	1 / 2	16.7		0.25
	0.70 / 0.30	1 / 2	14.4		0.30
	0.40 / 0.60	1 / 2	11.3		0.38
	0.25 / 0.75	1 / 2	9.27		0.49
ZrO ₂ C / Al ₂ O ₃ G	0.90 / 0.10	1 / 2	10.97 ± 0.58		0.39 ± 0.02
	0.80 / 0.20	1 / 2	11.43 ± 0.61		0.38 ± 0.02
	0.70 / 0.30	2 / 2	10.93 ± 1.44		0.41 ± 0.06
	0.60 / 0.40	1 / 2	10.67 ± 0.59		0.41 ± 0.03
	0.25 / 0.75	1 / 2	10.36 ± 0.14		0.44 ± 0.01
ZrO ₂ G / Al ₂ O ₃ C	0.90 / 0.10	2 / 2	7.30 ± 3.01		0.65 ± 0.23
	0.70 / 0.30	2 / 2	2.60 ± 0.64		1.87 ± 0.54
	0.50 / 0.50	1 / 2	1.53 ± 0.05		3.36 ± 0.17
	0.30 / 0.70	1 / 2	1.28 ± 0.09		4.04 ± 0.43
	0.10 / 0.90	1 / 2	1.19 ± 0.04		4.46 ± 0.31
ZrO ₂ C / Al ₂ O ₂ C	0.90 / 0.10	1 / 2	6.31 ± 1.29		0.70 ± 0.16
	0.80 / 0.20	1 / 2	2.84 ± 0.33		1.71 ± 0.26
	0.70 / 0.30	1 / 2	2.88 ± 0.35		1.58 ± 0.23
	0.60 / 0.40	1 / 2	1.89 ± 0.17		2.58 ± 0.31
	0.50 / 0.50	1 / 2	1.50 ± 0.17		3.43 ± 0.56
ZrO ₂ G / Y ₂ O ₃ C	0.70 / 0.30	1 / 2	3.00 ± 0.02		1.52 ± 0.03
ZrO ₂ C / Al ₂ O ₃ G / Y ₂ O ₃ C	0.34 / 0.33 / 0.10	1 / 3	5.11 ± 0.08		0.91 ± 0.01
	0.45 / 0.45 / 0.10	1 / 3	2.31 ± 0.06		2.15 ± 0.08

Table 5.

Powder	Type of milling (number of rotations)	Flow function coefficient ff_c (-)	Cohesion c (kPa)
Al ₂ O ₃ G	B01 (25 rotations)	8.26 ± 0.14	0.55 ± 0.02
Al ₂ O ₃ G	B02 (100 rotations)	4.43 ± 0.21	1.03 ± 0.07
Al ₂ O ₃ G	B03 (200 rotations)	2.79 ± 0.33	1.71 ± 0.26
ZrO ₂ C	B01 (25 rotations)	2.41 ± 0.01	1.96 ± 0.02
ZrO ₂ C	B02 (100 rotations)	1.45 ± 0.03	3.55 ± 0.02
ZrO ₂ C	B03 (200 rotations)	1.29 ± 0.00	4.00 ± 0.00
ZrO ₂ C / Al ₂ O ₃ G (0.7/0.3)	B01 (25 rotations)	3.14 ± 0.04	1.48 ± 0.01
ZrO ₂ C / Al ₂ O ₃ G (0.7/0.3)	B02 (100 rotations)	1.86 ± 0.02	2.56 ± 0.02
ZrO ₂ C / Al ₂ O ₃ G (0.5/0.5)	B02 (100 rotations)	1.99 ± 0.07	2.45 ± 0.01
ZrO ₂ C / Al ₂ O ₃ G (0.7/0.3)	B03 (200 rotations)	1.51 ± 0.02	3.24 ± 0.12

Martin GIRAUD (conceptualization, methodology, formal analysis, investigation, data curation, writing-original draft), Cendrine GATUMEL (supervision, validation), Stéphane VAUDEZ (supervision, validation), Guillaume BERNARD-GRANGER (supervision, validation), Jeremy NOS (validation), Thierry GERVAIS (validation), Henri BERTHIAUX (supervision, validation, writing-review and editing)

Highlights:

- A predictive model for the flowability of powder mixtures is built
- The mixtures are prepared either in a Turbula® mixer or in a ball mill
- Interparticle forces are investigated through the granular Bond number
- The Bond number accounts for particle size polydispersity of real powders
- Model predicts the flow behavior of the mixtures according to their compositions

Particle A

Particle B

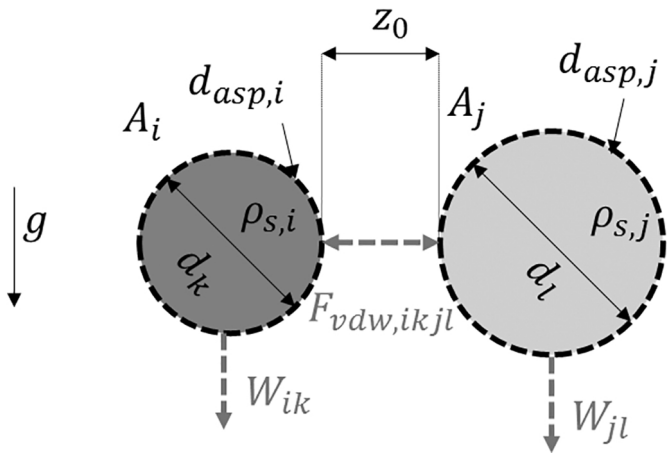


Figure 1

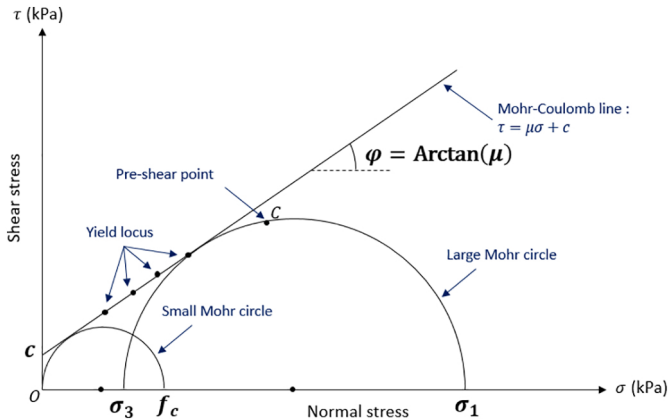


Figure 2

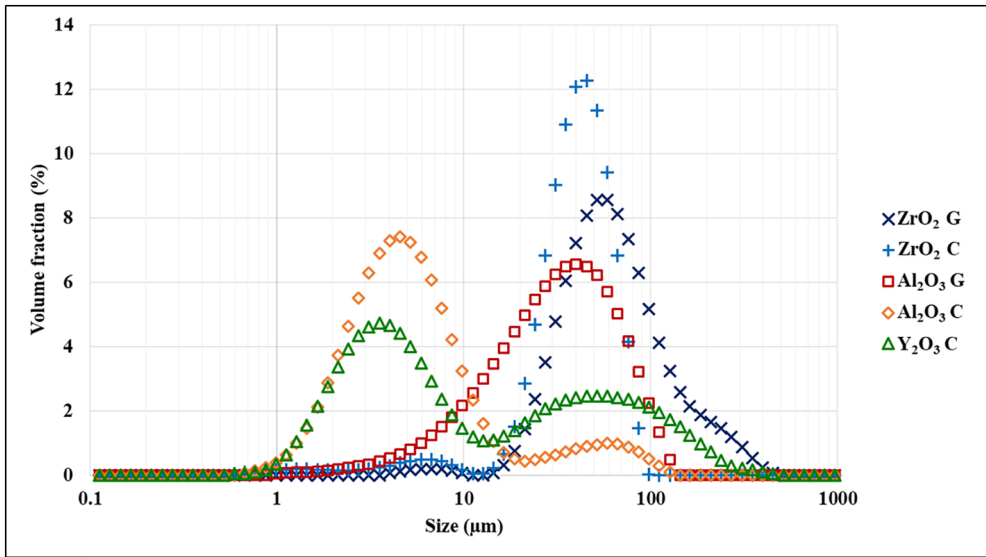


Figure 3

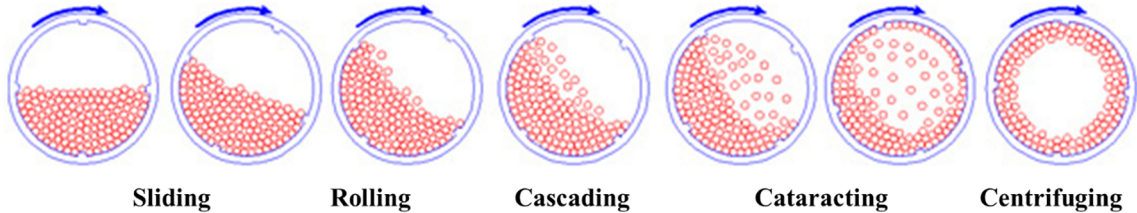
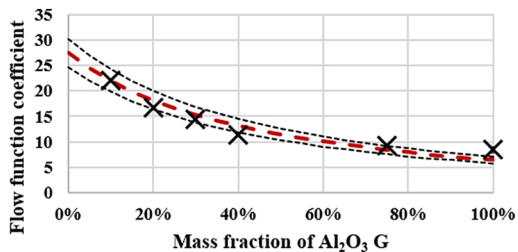
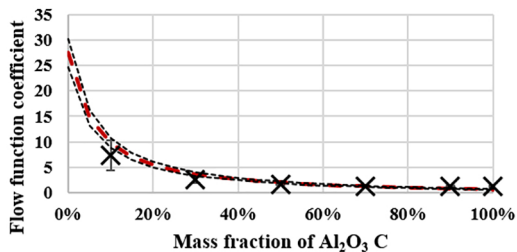


Figure 4

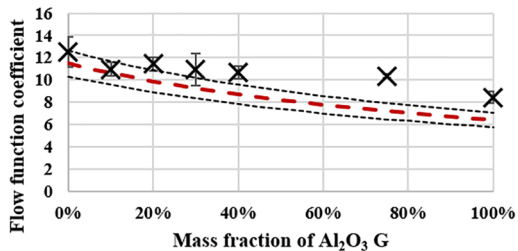
Binary mixture ZrO_2 G / Al_2O_3 G



Binary mixture ZrO_2 G / Al_2O_3 C



Binary mixture ZrO_2 C / Al_2O_3 G



Binary mixture ZrO_2 C / Al_2O_3 C

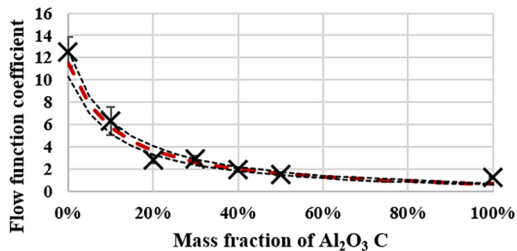


Figure 5

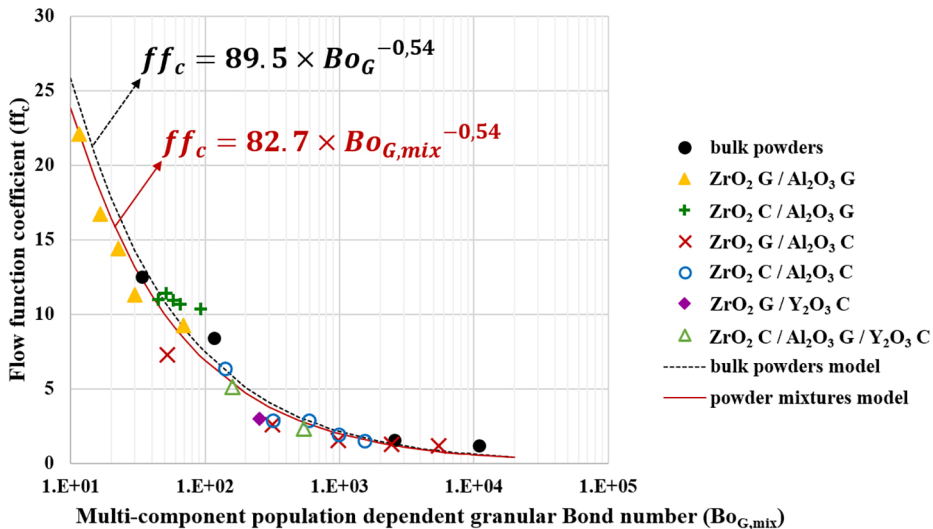
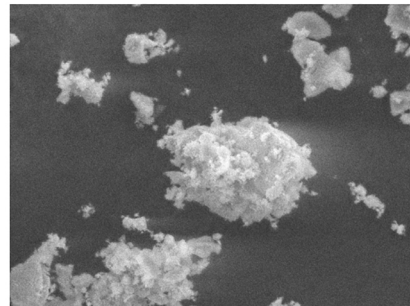
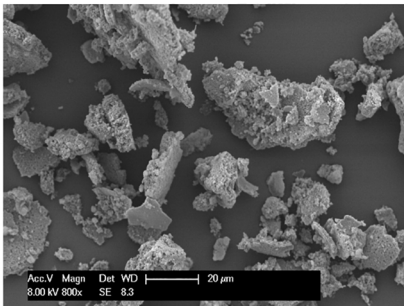


Figure 6

Bulk powders

Milled powders (B02)

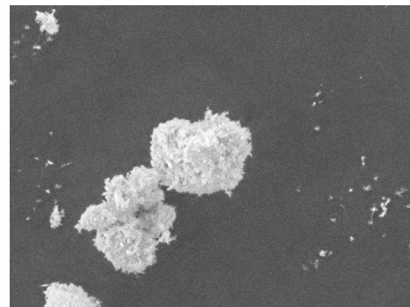
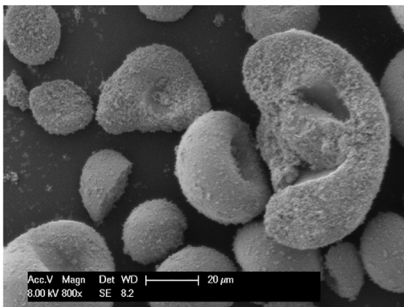
Al_2O_3 G



AG-B02-0002

NMUD8.2 x800 100 μm

ZrO_2 C



ZC-B02-0002

NMUD8.4 x800 100 μm

Figure 7

ZrO₂ C

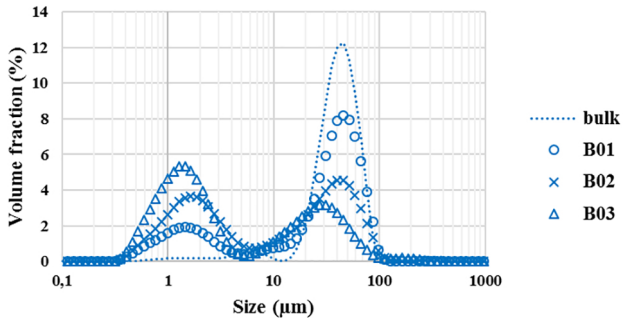


Figure 8

Al₂O₃ G

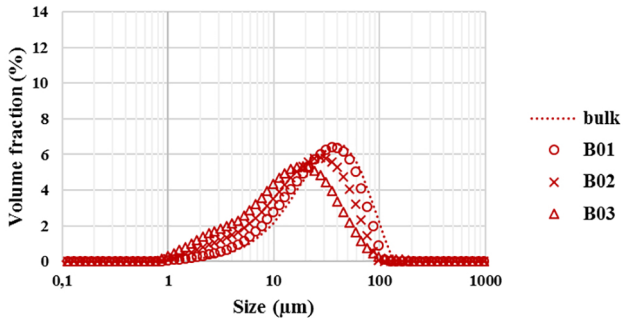


Figure 9

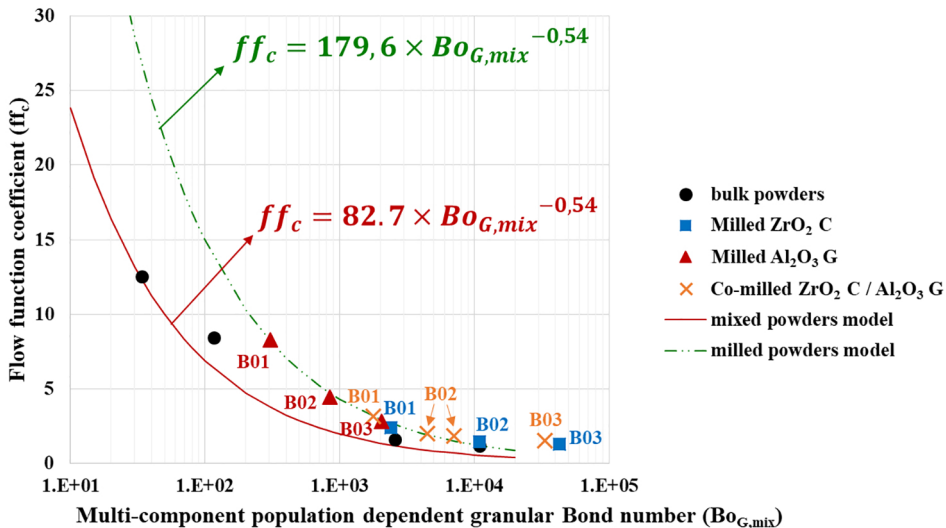
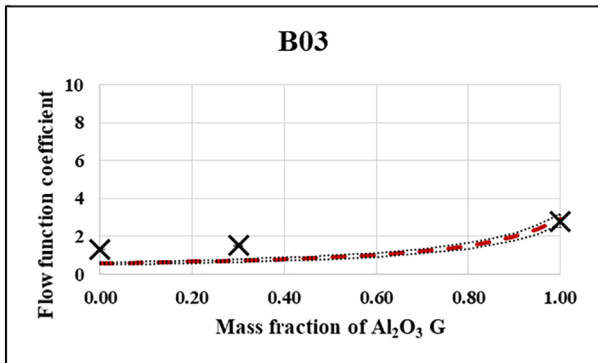
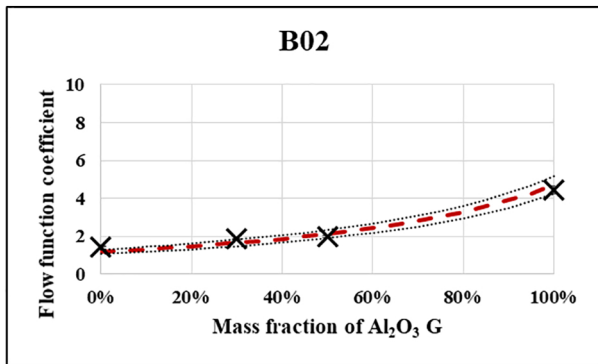
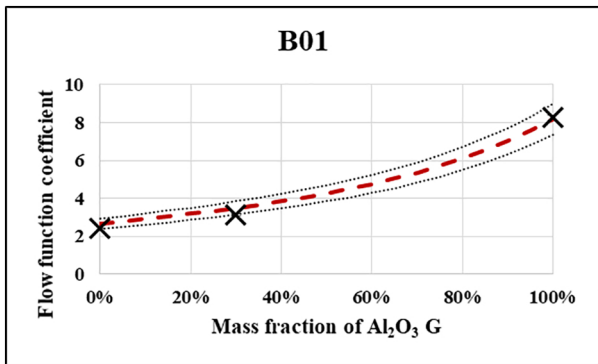


Figure 10



Co-milling of ZrO_2 C and Al_2O_3 G powders

B01: 1 minute (25 rotations)

B02: 4 minutes (100 rotations)

B03: 8 minutes (200 rotations)

Figure 11